AD-A109 934 CALIFORNIA UNIV LOS ANGELES CENTER FOR PLASMA PHYSIC--ETC F/G 20/9
PONDEROMOTIVE POTENTIAL NEAR GYRORESONANCE,(U)
NOV 81 G DIMONTE, B M LAMB, G J MORALES N00014-75-C-0476
UNCLASSIFIED PPG-594 NL

END
DATE FILMED
3-82
DTIC

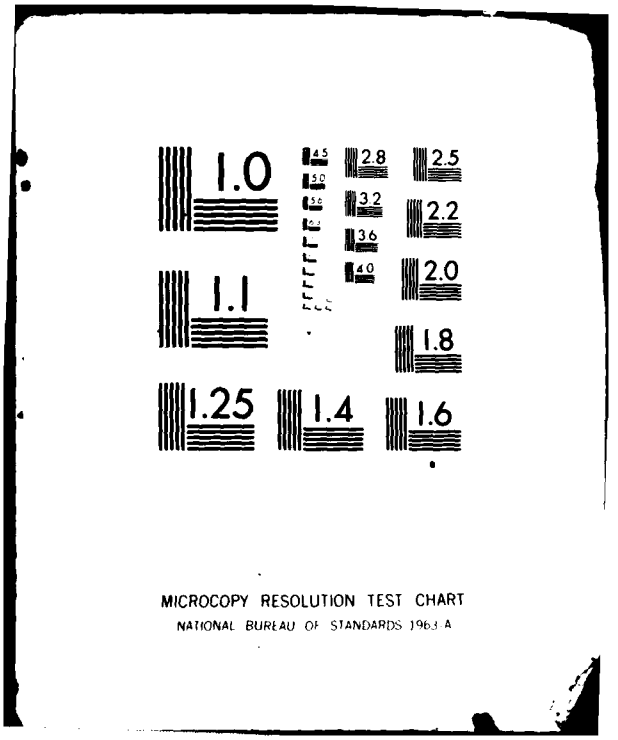
1.0
1.1
1.25
1.4
1.6
1.8
2.0
2.2
2.5
2.8
3.2
3.6
4.0
4.5
5.0
MICROCOPY RESOLUTION TEST CHART
NATIONAL BUREAU OF STANDARDS 1963-A

CENTER FOR
PLASMA PHYSICS
AND
FUSION ENGINEERING

UNIVERSITY OF CALIFORNIA
LOS ANGELES

Ponderomotive Potential Near Gyroresonance

Guy Dimonte, B. M. Lamb & G. J. Morales

Contract N00014-75-C-0476

PPG-594 ✓ November, 1981

Department of Physics
University of California, Los Angeles
Los Angeles, California 91604

It is known that a spatially localized rf electric field $\underset{\sim}{E}$ of frequency ω produces an average static force, i.e., a ponderomotive force.[1] In the presence of a static magnetic field $\underset{\sim}{B}$ a large enhancement of the ponderomotive force is predicted[2] to appear as ω approaches the particle gyrofrequency Ω. The standard expression[2] given for the ponderomotive (pseudo) potential is

$$\phi_p = \frac{q^2 \ |\underset{\sim}{E}|^2}{4m(\omega^2 - \Omega^2)} \tag{1}$$

where q and m are the charge and mass of the particle. The non-physical singularity in Eq. (1) arises because in obtaining this expression the gradient scale length ℓ of the electric field is assumed to be large compared to $v/(\omega - \Omega)$, where v is the unperturbed particle velocity. However, this adiabatic approximation[3] is not valid near gyroresonance, hence the singularity in Eq. (1) is suspect. Since the ponderomotive force plays a fundamental[4] role in many nonlinear processes in plasma physics, it is important to understand the singular behavior near the gyrofrequency. In particular, efforts are in progress to utilize the singular nature of ϕ_p to selectively confine ions of different q/m for isotope separation[5-6] and to plug open ended confinement systems.[7-8]

In this Letter, we present measurements of the ponderomotive potential near gyroresonance and compare them with a calculation which includes nonadiabatic effects. It is found, both experimentally and theoretically, that ϕ_p is vanishingly small at $\omega = \Omega$ rather than singular. In fact, the maximum enhancement in ϕ_p does not occur at $\omega = \Omega$, but at the transition from the nonadiabatic to the adiabatic regime, namely, for $\omega \simeq \Omega + 1.7v/\ell$.

The experiment is performed by injecting a low density (single particle limit) monoenergetic pulse of ions through an electrostatic rf structure as

shown in Fig. 1. The rf electric field amplitude is increased until the transmitted current disappears. At this point ϕ_p is equal to the kinetic energy $mv^2/2$ of the particles. Experimentally one must be extremely careful that the decrease in current arises because the particles are reflected by the ponderomotive force rather than being scraped off by the antenna as a result of cyclotron heating. The ion source is a thermionic emitter capable of producing $^7Li^+$ and $^{27}A\ell^+$ simultaneously. A pulse of ions of energy $q\,V_S$, where V_S is the source bias voltage, is produced by gating a grid from $V > V_S$ to $V = 0$ for a duration of 20μ s. The ions are guided along the axis of a grounded conducting cylinder by a uniform axial magnetic field B_o = 1.8 Kg. The beam radius is 0.5 cm, and the cylinder radius is 7.3 cm. The rf antenna consists of two electrically isolated electrodes made by splitting a cylinder in half lengthwise. It is excited through a center tapped transformer so that $\underset{\sim}{E}$ is perpendicular to $\underset{\sim}{B}$ on axis. We have calculated the vacuum rf field $\underset{\sim}{E}(r, \theta, z)$ analytically to relate $\underset{\sim}{E}$ to the rf potential $\pm V_{rf}$ applied to the electrodes. On axis, the field has a Gaussian profile $\underset{\sim}{E}(r = 0, \theta, z) = \hat{y}\, E_o \exp(-z^2/2\ell^2)$ with scale length ℓ which can be varied by changing the length of the antenna. The ions which pass through the antenna are collected by an electrode which is 137 cm away from the source.

Figure 2 demonstrates the mass selectivity of the ponderomotive force as well as the distinction between true ponderomotive stopping and fake current drop caused by resonance heating. The time dependence of the collected ion current is shown for various conditions. Since all emitted ions have the same energy the arrival time for each species depends on the mass m. Without rf the signal exhibits two peaks, one corresponding to m = 7 ($^7Li^+$) and the other m = 27 ($^{27}A\ell^+$). When the rf pulse is applied at the gyrofrequency of m = 7, i.e., $\omega = \Omega_7$, the Li peak disappears and the Aℓ peaks remain unaffected

($\omega > \Omega_{27}$). The drop in Li current is not a ponderomotive effect, but rather is the manifestation of ion cyclotron heating. Our measurements indicate that the orbits become so large that the particles are scraped-off by the antenna structure. When the frequency is increased to $\omega = 1.5\ \Omega_7$, as seen in Fig. 2, the early peak (Li) disappears once again, but now an additional peak appears just after the rf is turned off. These ions are reflected twice, first by the ponderomotive potential at the antenna, and then by the gate grid at the entrance end of the device. The area under the additional peak indicates that 90% of the Li ions are confined by the rf. The Aℓ peak is unaffected because $\omega >> \Omega_{27}$ indicating the mass selectivity of the ponderomotive force. Similar mass selection occurs near Ω_{27}.

The ponderomotive potential is measured for a fixed value of ω, Ω, ℓ and v by increasing V_{rf} until the transmitted ion current disappears. For this value of V_{rf} the ponderomotive potential equals the initial kinetic energy. If the gyrofrequency enhancement of the ponderomotive potential is large then a relatively small rf electric field is required to reflect the particles and vice versa. Data for which there are no trapped ions are discarded because the previously described scrape-off would influence the measurement. The initial kinetic energy of the ions is $qV_s \pm 15\%$ as verified by time-of-flight analysis and retarding field analyzer measurements. The electric field amplitude on axis E_o is obtained from V_{rf} by using our analytical solutions for the vacuum field. This is justified because the ion density is purposely small to minimize space charge effects. The gradient scale length ℓ is also obtained from these calculations since the antenna radius and length are known.

Figure 3 shows the behavior of the ponderomotive potential near the gyrofrequency. ϕ_p is scaled to $q^2E_o^2/4m\Omega^2$ as suggested by Eq. (1) to fa-

cilitate comparison of the data (dots) with the theoretical predictions (solid curves). The curve for $v/\ell\Omega = 0$ is given by Eq. (1) and the rest will be described later. Five sets of data for different values of ℓ and v are shown to demonstrate the important parametric dependences. Away from gyroresonance ϕ_p agrees quantitatively with the prediction of Eq. (1) whereas near Ω the data disagrees even qualitatively; ϕ_p reaches a maximum at a frequency greater than Ω and tends toward a small value at Ω. There are three sets of data which have the same value of $v/\ell\Omega$ but different values of ℓ and v. These data agree with one another within the experimental error indicating that the relevant parameter is $v/\ell\Omega$. By obtaining data over a wide range of parameters, we find that the maximum in ϕ_p occurs at a frequency $\omega \simeq \Omega + 1.7\ v/\ell$. As a result, the maximum enhancement of the ponderomotive potential depends on various parameters through the figure of merit $v/\ell\Omega$; the implication is that in order to obtain a significant enhancement of the ponderomotive force near gyroresonance $v/\ell\Omega$ must be small.

To explain these results it is necessary to integrate the equation of motion properly as a particle traverses an electric field structure of finite extent. Consider the exact equation of motion for a particle with position $\underset{\sim}{r}$ in the magnetic field $\underset{\sim}{B} = B_o\hat{z}$

$$\ddot{\underset{\sim}{r}} = \frac{q}{m}\underset{\sim}{E}(\underset{\sim}{r},t) + \Omega\dot{\underset{\sim}{r}} \times \hat{z} \qquad (2)$$

For simplicity, assume that $\underset{\sim}{E} = (E_y(y,z)\hat{y} + E_z(y,z)\hat{z})\cos(\omega t + \psi)$ where ψ is a phase factor and $\nabla \times \underset{\sim}{E} = 0$. We proceed to solve Eq. (2) by employing a multiple time scale perturbation expansion $\underset{\sim}{r}(t) = \underset{\sim}{r}_s(t) + \underset{\sim}{r}_f(t)$ where $\underset{\sim}{r}_f$ gives the fast response of the particle and $\underset{\sim}{r}_s$ varies on a slow time scale (compared to $2\pi/\omega$). By expanding $\underset{\sim}{E}(\underset{\sim}{r}, t)$ about $\underset{\sim}{r}_s$ assuming $|\underset{\sim}{r}_f| \ll \ell$ and equating terms of similar time scales we obtain

$$\ddot{\underset{\sim}{r}}_f = \frac{q}{m} \underset{\sim}{E} (\underset{\sim}{r}_s, t) + \Omega \dot{\underset{\sim}{r}}_f \times \hat{z} \tag{3}$$

where $\underset{\sim}{E}(\underset{\sim}{r}_s,t)$ is evaluated at the average location $\underset{\sim}{r}_s$. The slow response of the particle is determined by the static ponderomotive force

$$\underset{\sim}{F}_p = q \langle (\underset{\sim}{r}_f \cdot \underset{\sim}{\nabla}) \underset{\sim}{E}(\underset{\sim}{r}_s, t) \rangle \tag{4}$$

where the brackets denote an average over the fast-time scale $2\pi/\omega$. The parallel component responsible for stopping the particle has two contributions $\langle q y_f \frac{d}{dy} E_z \rangle$ and $\langle q\, z_f \frac{d}{dz} E_z \rangle$. The latter gives the usual unmagnetized contribution[1] which is not of interest here and is quite small in our experiment because $E_z = 0$ on axis ($y = 0$) where the particles are injected. Using $\underset{\sim}{\nabla} \times \underset{\sim}{E} = 0$ the first term becomes $\langle q\, y_f \frac{d}{dz} E_y \rangle$. To evaluate this we solve for y_f by integrating Eq. (3)

$$y_f = \frac{q}{m\Omega} \int_{-\infty}^{t} dt'\, E_y\, (0,\, z_s(t'))\sin\,(\Omega(t - t'))\cos(\omega t' + \psi) \tag{5}$$

In the adiabatic limit $\ell(\omega - \Omega)/v \gg 1$, $E_y\,(0,\, z_s)$ can be removed from the integral, y_f becomes singular and the standard result, i.e., Eq. (1), is recovered. However, near gyroresonance E_y must be retained inside the time history integral. In general, Eq. (5) is diffifult to solve, hence we make the simplification that $z(t) = vt\,\hat{z}$. That is, we integrate over the unperturbed particle orbit retaining E_y inside the integral. We shall return to this point later. Substituting y_f into Eq. (4) and defining the ponderomotive (pseudo) potential as $\phi_p(o,z) \equiv -\int_{-\infty}^{z} dz'\, \underset{\sim}{F}_p\,(o,z') \cdot \hat{z}$ we obtain

$$\phi_p(0,z) = \frac{q^2 E_y^2(0,z)}{8m\omega(\omega + \Omega)} - \frac{q^2 E_y(0,z)}{4m\omega v}\, \mathrm{Im}\,\xi - \frac{q^2(\omega - \Omega)}{8m\omega v^2}|\xi|^2 \tag{6}$$

where Im refers to the imaginary part and

$$\mathcal{E} \equiv \int_{\infty}^{z} dz' \, E_y(0, z') \exp\left[i(\omega - \Omega)(z' - z)/v\right] \qquad (7)$$

In the adiabatic limit $(\omega - \Omega)\, \ell/v >> 1$, Eq. (6) reduces to Eq. (1). Otherwise the strength of the potential has an additional dependence on the electric field profile and the velocity of the particle.

Using a Gaussian profile for E_y in Eq. (6) gives an analytical expression for $\phi_p(o,z)$ in terms of the plasma dispersion function.[9] Proceeding to identify $\phi_p(0,0)$ with the maximum stopping power measured in the experiment, one arrives at the solid curves exhibited in Fig. 3. The agreement between the calculation and the experimental values is excellent. This result also agrees with previous rf plugging experiments[7-8] in which the maximum stopping power of the ponderomotive force occured at frequencies above the gyrofrequency.

It is illustrative to evaluate $\phi_p(0,0)$ for the Gaussian profile near gyroresonance, i.e., $(\omega - \Omega)\ell/v << 1$,

$$\phi_p(0,0) \simeq \frac{q^2 E_o^2}{8m\omega(\omega+\Omega)} + \frac{q^2 E_o^2 \ell^2}{4m\omega v^2}(1 - \pi/4)(\omega - \Omega) \qquad (8)$$

which is finite. The first term is small and arises from the nonresonant polarization of the antenna, i.e., the rf field is linearly polarized. The second term arises from the resonant polarization and vanishes exactly at gyroresonance. Physically this occurs because the transit time ℓ/v is very short compared to the time required for the particle to see a change in the relative phase of the perpendicular rf electric field, i.e., $(\omega - \Omega)^{-1}$. Consequently, the particle response depends on the phase of the electric field when it enters the rf structure. In this case, the notion of a time independent conservative force breaks down and stochastic particle heating occurs.[10] This effect is included in the solution of Eq. (3) and manifests itself through the integral $\mathcal{E}$ appearing in Eq. (7).

It is somewhat surprising that there is such good agreement between theory and experiment because our calculation, as well as the adiabatic calculation,[1-3] uses the Born approximation. This assumes that the high frequency response of the particle can be calculated by integrating the equation of motion along the unperturbed orbit; a condition which is violated in rf plugging experiments including ours because the particles are reflected at some point. To further validate the perturbation results we have calculated the exact particle orbits numerically using a Gaussian profile for the electric field. The stopping potential is also found to be in close agreement with Eq. (6).

In summary, a second order perturbation calculation illustrates the finite nature of the ponderomotive effect near the gyroresonance and is in excellent agreement with detailed experimental observations with test ions. Near the gyrofrequency the ponderomotive potential is a function not only of position but also depends on the velocity of the particles.

This research was supported by the Office of Naval Research (B. M. L. and G. J. M.) and by the National Science Foundation (G. D.) under grant NSF PHY79-08480.

References

1. A. V. Gaponov and M. A. Miller, ZhETF 34, 242 (1958) [Sov. Physics JETP 7, 168 (1958).]
2. L. P. Pitaevskii, J. Exptl. Theoret. Phys. 39, 1450 (1960) [Sov. Physics JETP 12, 1008 (1961).]
3. A. J. Lichtenberg and H. L. Berk, Nuclear Fusion 15, 999 (1975).
4. J. R. Cary and A. N. Kaufman, Phys. Fluids 24, 1238 (1981).
5. S. Hidekuma, S. Hiroe, T. Watari, T. Shoji, T. Sato, and K. Takayama, Phys. Rev. Lett. 33, 1537 (1974).
6. E. S. Weibel, Phys. Rev. Lett. 44, 377 (1980).
7. S. Hiroe, S. Hidekuma, T. Watari, T. Shoji, T. Sato, and K. Takayama, Nuclear Fusion 15, 769 (1975).
8. T. Watari, T. Hatori, R. Kumazawa, S. Hidekama, T. Aoki, T. Kawamoto, M. Inutake, S. Hiroe, A. Nishizawa, K. Adati, T. Sato, T. Watanabe, H. Obayashi, and K. Takayama, Phys. Fluids 21, 2076 (1978).
9. B. D. Fried and S. Conte, The Plasma Dispersion Function, (Academic, New York, N.Y. 1961).
10. G. J. Morales and Y. C. Lee, Phys. Rev. Lett. 33, 1534 (1974).

Figure Captions

Figure 1 Schematic of the experiment.

Figure 2 Collected ion current versus delay time for three conditions of the rf field. Ion energy is 10 ev.

Figure 3 Scaled ponderomotive potential versus frequency for different conditions. Dots are measured and the curves are the theoretical predictions. The curve for $v/\ell\Omega = 0$ is given by Eq. (1).

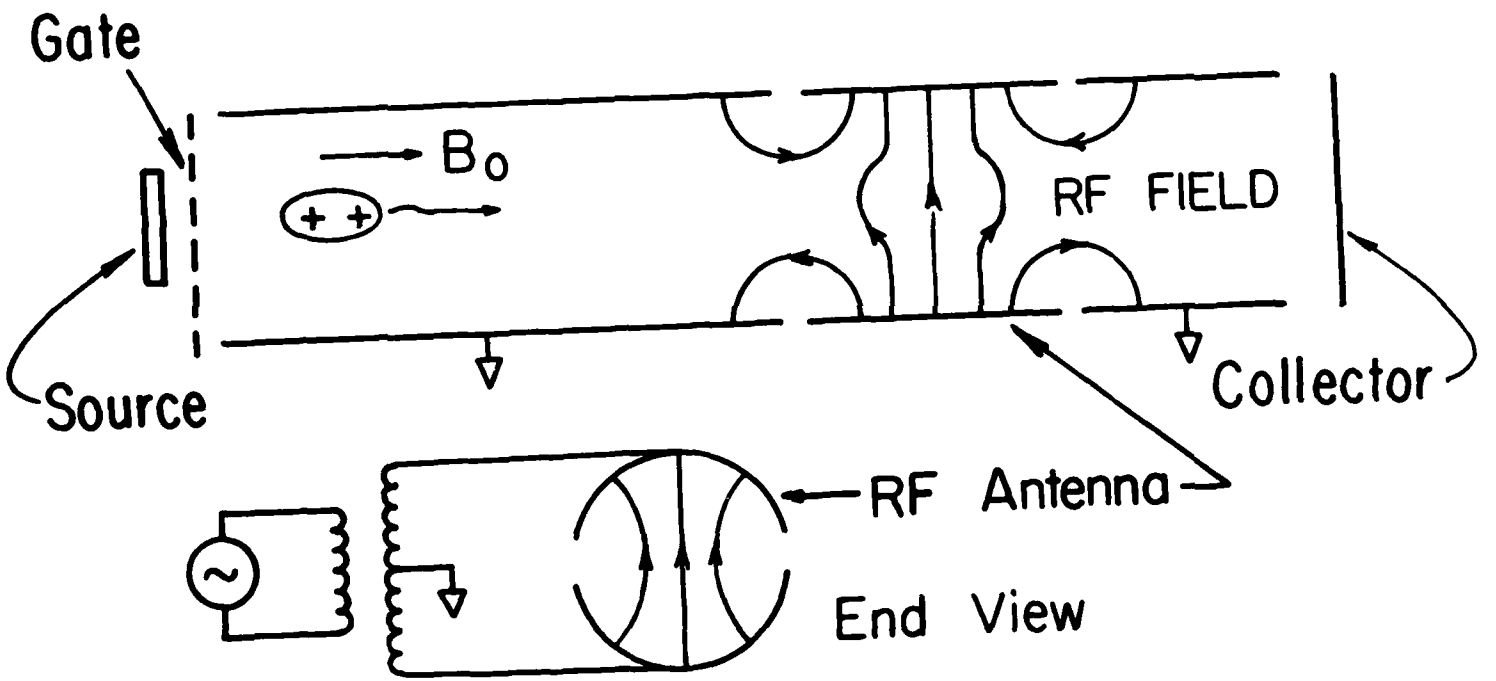

FIG. 1

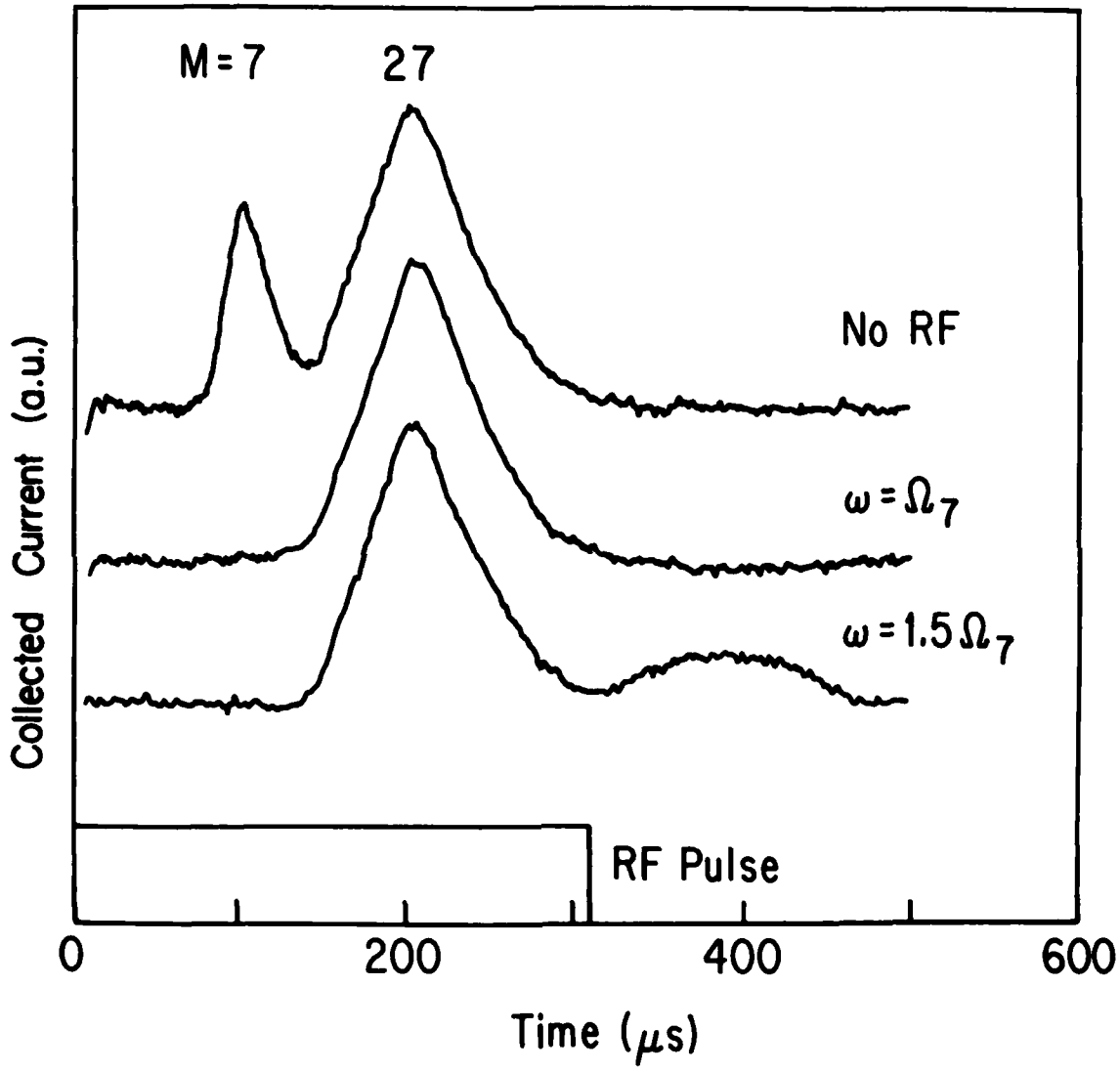
M=7
27
No RF
ω=Ω7
ω=1.5Ω7
Collected Current (a.u.)
RF Pulse
0
200
400
600
Time (μs)

FIG. 2

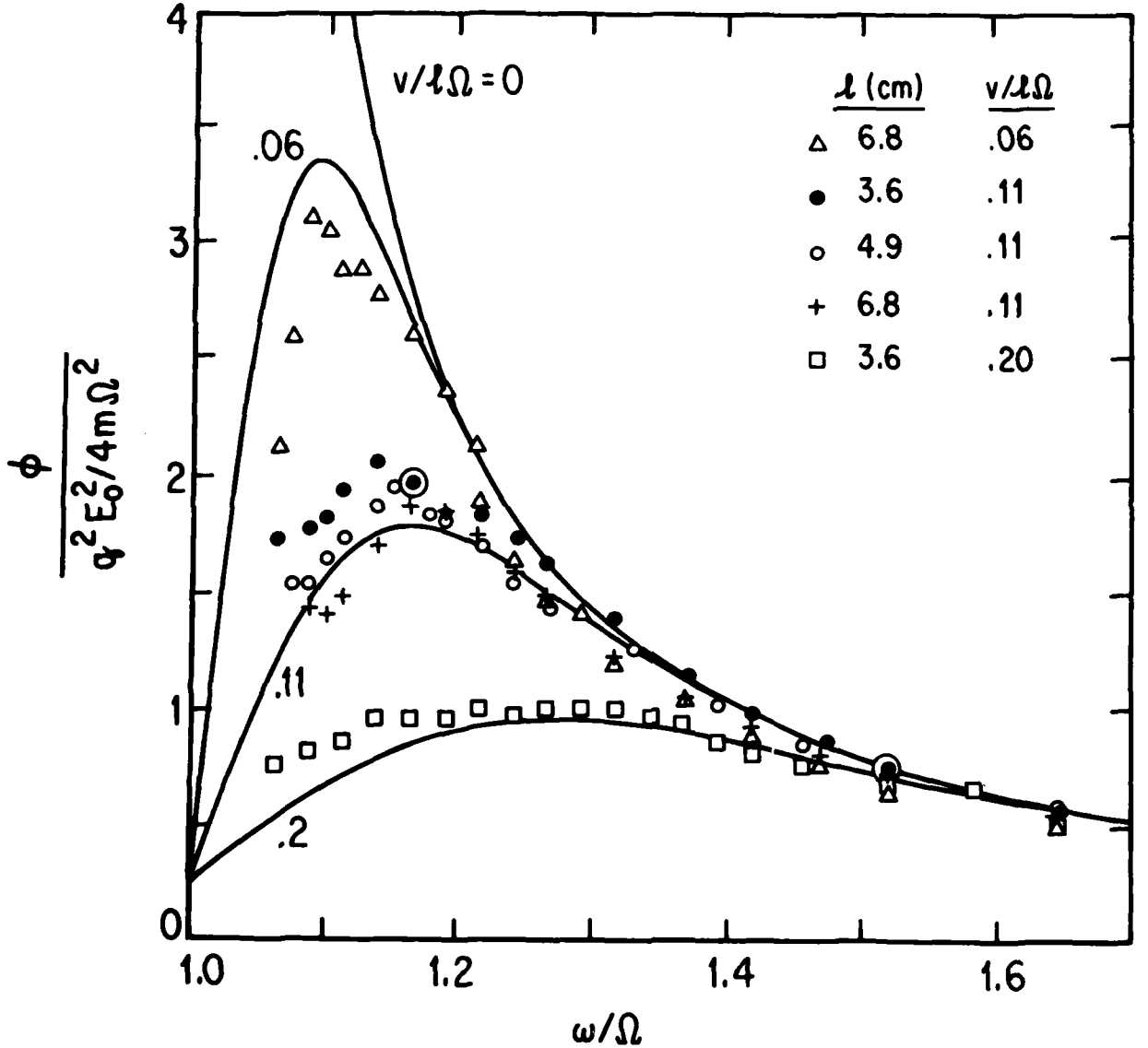
4
3
2
1
0
1.0
1.2
1.4
1.6
ω/Ω
$\frac{\phi}{q^2E_o^2/4m\Omega^2}$
v/ℓΩ = 0
.06
.11
.2
ℓ (cm)
v/ℓΩ
△ 6.8 .06
● 3.6 .11
○ 4.9 .11
+ 6.8 .11
□ 3.6 .20

FIG. 3

PPG-566 "Far Infrared Laser Scattering Studies of Density Fluctuations in Tokamak Fusion Plasmas," P. Lee, N.C. Luhmann, H. Park, W.A. Peebles, R.J. Taylor, and C.X. Yu, June (1981).

PPG-567 "Energy Transport in Hot Electron Microexplosions Driven by a CO_2 Laser," C. Joshi, N.H. Burnett, and N.A. Ebrahim, June (1981).

PPG-568 "Resonance Absorption Produced Hot Electrons in a Microwave Plasma Interaction," A.Y. Lee, Y. Nishikawa, N. Luhmann, S.P. Obenschain, B. Gu, and M. Rhodes, June (1981).

PPG-569 "EXPRESS: A Computer Code to Study Helium Behavior in Inertial Confinement Fusion Reactor Structural Materials," R. Schafer and Nasr-Ghoniem, July (1981).

PPG-570 "A Note on Compton Scattering," D.D. Barbosa, July (1981).

PPG-571 "Magnetosonic Wave Heating of High Beta Plasmas," K. Nozaki, B.D. Fried, and G.J. Morales, July (1981).

PPG-572 "New York Abstracts, Papers for the New York Meeting on the Division of Plasma Physics, American Physical Society," July (1981).

PPG-573 "Energy Conservation Theorem for Electrostatic Systems," V.K. Decyk, August (1981).

PPG-574 "Finite Temperature Relativistic Magnetohydrodynamic Winds," F.S. Fujimura and C.F. Kennel, August (1981).

PPG-575 "D-D Tandem Mirror Reactor Analysis and Requirements," F. Kantrowitz and R.W. Conn, September (1981).

PPG-576 "SATYR Studies of a D-D Fueled Axisymmetric Tandem Mirror Reactor," R.W. Conn, et. al., September (1981).

PPG-577 "Observation of Mode Converted Electrostatic Waves in the ICRF Region in the Microtor Tokamak," P. Lee, et. al., September (1981).

PPG-578 "MHD Stability and Confinement in a Large Diameter, Axisymmetric Mirror with High Mirror Ratio," J. R. Ferron, A. Y. Wong, P. Young, B. Leikind, G. Dimonte, September (1981).

PPG-579 "Linear and Nonlinear Behavior of DCLC Mode in a Large Diameter, Axisymmetric Magnetic Mirror," J. R. Ferron and A. Y. Wong, September (1981).

PPG-580 Save for Art Walstead

PPG-581 Save for Allen Adler

PPG-582 "Efficient, Higher Order Griding Center Calculations Via the Action Form $\underset{\sim}{p}\cdot d\underset{\sim}{q}-Hdt$," R. G. Littlejohn, September (1981).

PPG-583 "Ion Heating and Confinement in the UCLA Toroidal Cusp Experiment," M. Rhodes, J. M. Dawson, J. N. Leboeuf, and N. C. Luhmann, Jr., September (1981).

PPG-584 "Laboratory Experiments on Magnetic Field Line Reconnection," R. Stenzel and W. Gekelman, October (1981).

PPG-585 "Relation of Surface Interactions to First-Wall and In-Vessel Component (IVC) Design and Materials Performance in Fusion Devices," R. Conn, October (1981).

PPG-586 "The Satyr Study of d-d Cycle Tandem Mirror Reactors," R. Conn, et al., October (1981).

PPG-587 "Assessment of Ferritic Steels for Steady-State Fusion Reactors," N. Ghoniem, R. Conn, October (1981).

PPG-588 "Mission, Concept, and Objectives of the Fusion Engineering Device (FED)," R. Conn, et al., October (1981).

PPG-589 "Studies of the Physics and Engineering of D-D Barrier Tandem Mirror Reactors," R. Conn, October (1981).

PPG-590 "Electrostatic Wave Propagation and Trapping Near the Magnetic Equator," D. D. Barbosa, October (1981).

PPG-591 "Simultaneous Observation, Spikey Turbulence and Electromagnetic Radiation," P. Y. Cheung, A. Y. Won, C. B. Darrow, S. J. Quian, October (1981).

PPG-592 "Generation of Non-Thermal Continuum Radiation in the Magnetosphere," H. Okuda, M. Ashour-Abdalla, M. S. Chance, and W. S. Kurth, November (1981).

PPG-593 "Fusion Product Energy and Particle Loss from Tandem-Mirror Reactors by Nuclear Scattering," F. Kantrowicz and R. W. Conn, November (1981).

PPG-594 "Ponderomotive Potential Near Gyroresonance," G. Dimonte, G. J. Morales, and B. M. Lamb, November (1981), submitted to Phys. Rev. Lett.


8
DTIC